Rock Mech Rock Eng (2017) 50:309–326
DOI 10.1007/s00603-016-1110-1

ORIGINAL PAPER

Estimation of Confined Peak Strength of Crack-Damaged Rocks

Navid Bahrani[1] · **Peter K. Kaiser**[2]

Received: 11 December 2015 / Accepted: 4 October 2016 / Published online: 22 October 2016

Abstract It is known that the unconfined compressive strength of rock decreases with increasing density of geological features such as micro-cracks, fractures, and veins both at the laboratory specimen and rock block scales. This article deals with the confined peak strength of laboratory-scale rock specimens containing grain-scale strength dominating features such as micro-cracks. A grain-based distinct element model, whereby the rock is simulated with grains that are allowed to deform and break, is used to investigate the influence of the density of cracks on the rock strength under unconfined and confined conditions. A grain-based specimen calibrated to the unconfined and confined strengths of intact and heat-treated Wombeyan marble is used to simulate rock specimens with varying crack densities. It is demonstrated how such cracks affect the peak strength, stress–strain curve and failure mode with increasing confinement. The results of numerical simulations in terms of unconfined and confined peak strengths are used to develop semi-empirical relations that relate the difference in strength between the intact and crack-damaged rocks to the confining pressure. It is shown how these relations can be used to estimate the confined peak strength of a rock with micro-cracks when the unconfined and confined strengths of the intact rock and the unconfined strength of the crack-damaged rock are known. This approach for estimating the confined strength of crack-damaged rock specimens, called strength degradation approach, is then verified by application to published laboratory triaxial test data.

Keywords Micro-crack · Confined strength · Strength Degradation Approach (SDA) · Particle Flow Code (PFC) · Grain-based Model (GBM) · Confidence Interval (CI)

1 Introduction

Reliable design of structures in rock requires reliable estimates of rock mass strength, a strength that is influenced by the presence of geological features at various scales (i.e., micro-cracks and cracks at the laboratory specimen scale, fractures and veins at the rock block scale, and block-forming joints at the rock mass scale). The determination of the strength of rock at the laboratory specimen scale is the first step in the process of estimating the rock mass strength.

It is well known that the presence of micro-cracks[1] in the form of grain or grain boundary micro-cracks reduces the unconfined compressive strength of laboratory-scale specimens. Griffith (1921) proposed that the strength of brittle materials is strongly influenced by the presence of small cracks and that failure occurs when the most vulnerably oriented crack in a population of randomly oriented cracks grows under the applied stress. He also explained that very high tensile stresses can be generated at the tips of a pre-existing open crack even in an overall compressive stress condition and that can lead to initiation of new cracks

✉ Navid Bahrani
navidbahrani@yahoo.com

[1] Lassonde Institute of Mining, University of Toronto, Galbraith Building, 35 St. George Street, Toronto, ON M5S 1A4, Canada

[2] Bharti School of Engineering, Laurentian University, Sudbury, ON, Canada

[1] Definitions and adopted terminologies used in this article, such as intact rock, micro-crack, and strength degradation are provided in the "Appendix."

once the tensile stress on the boundary of the crack exceeds the local tensile strength of the material. Experimental evidence obtained by Hoek and Bieniawski (1965) showed that the crack length propagated from the tips of a pre-existing crack depends on the confinement. They found that the crack length under triaxial compression is sensitive to the ratio of σ_1/σ_3, where σ_1 and σ_3 are the major and minor principal stresses at failure, respectively, and that the crack length extension reduces to less than 10 % of its original length for confining pressures greater than about 10 % of the applied major principal stress.

Martin and Stimpson (1994) and Eberhardt et al. (1999) found that the observed decrease in the rock strength obtained from cores of the Lac du Bonnet (*LdB*) granite with increasing depth is due to an increase in the density of stress-induced micro-cracks. Watson et al. (2009) made a similar observation on specimens taken from deep mines in South Africa, and Lanaro et al. (2009) reported a strong negative correlation between rock strength and in situ stresses. Lanaro et al. (2009) related this observation to the presence of micro-cracks in the specimens taken from high-stress zones associated with faults. Holt et al. (2000) generated synthetic rocks cured under initial stress and applied an approximate coring stress path to generate damage in the form of micro-cracks in the specimens. The damaged specimens exhibited lower unconfined compressive strength than undamaged specimens. Hoek and Brown (1980) show how rock strength decreases with increasing the specimen size, and Hoek and Brown (1997) suggest that this reduction is due to the greater opportunity for failure along grain boundaries and through grains with pre-existing micro-cracks, as more and more of these features are included in the specimen. According to Hoek and Brown (1997), when a sufficiently large number of grains and micro-cracks are included in a specimen, the strength asymptotically approaches a constant, lower value.

The above-mentioned investigations were focused on the strength of rock specimens at the laboratory scale under unconfined conditions. A number of laboratory experiments investigated the influence of cracks on the confined strength of rock and observed a more rapid increase in its peak strength with increasing confinement compared to that of intact rock. Among them are Rosengren and Jaeger (1968) and Gerogiannopoulos (1976) who conducted triaxial tests on intact and heat-treated Wombeyan marble, which are discussed in more detail in this article.

In this article, two-dimensional distinct element models, previously calibrated to the unconfined and confined strengths of intact and heat-treated Wombeyan marble by Bahrani et al. (2014), are used to simulate rock specimens with varying degrees of crack density. The influence of micro-cracks, simulated in the form of grain boundary frictional cracks, on the strength and failure mode at various confinement levels is investigated. The results of these simulations are then used to develop semi-empirical relations for the estimation of the confined strength of rocks containing micro-cracks. The applicability of the proposed approach is compared to published laboratory triaxial test data.

2 Background

2.1 Properties of Intact and Granulated Wombeyan Marble

Rosengren and Jaeger (1968) and Gerogiannopoulos (1976) found that when a specimen of coarse-grained Wombeyan marble is heated to 600 °C, the anisotropy in thermal expansion of calcite grains causes complete separation of the grains at their boundaries. They mentioned that during heating, the specimen initially emitted "pinging" sounds, which were attributed to tensile failure of the grain boundaries and confirmed by microscopic examination showing open grain boundaries. The heat-treated (called granulated) marble had a low direct tensile strength of 0.03 MPa, compared to 7 MPa before heat treatment, supporting the interpretation of cohesionless grain boundaries after heat treatment.

Heating the marble reduced the unconfined compressive strength to about one quarter of its intact strength (from $UCS_i = 78$ MPa to $UCS_d = 20$ MPa; see Fig. 1a).[2] In the low confinement range ($\sigma_3 < \sim UCS_i/10$), the equivalent friction angle is 45° and 55° for the intact and heat-treated marble, respectively, as shown in Fig. 1a. Figure 1a also shows that, in the high confinement range ($\sigma_3 > \sim UCS_i/10 = 7$ MPa), the equivalent friction angles of intact and heat-treated marble are about 30°. Beyond this critical confining pressure (shown by arrows in Fig. 1a), most dilation is inhibited and the confined strength of granulated marble becomes about 80 % of the marble's intact strength.

Figure 1b shows the strength degradation (see "Appendix" for definition) of heat-treated Wombeyan marble ($\Delta\sigma_1 = \sigma_{1i} - \sigma_{1d}$) as a function of confinement. Up to a confining pressure of about $\sigma_3 = UCS_i/10$, the strength degradation of granulated marble decreases rapidly, and approaches an almost constant threshold value of about 10 MPa.

2.2 Grain-Based Model of Wombeyan Marble

Bahrani et al. (2014) used the two-dimensional Particle Flow Code (*PFC2D*) (Itasca 2008; Potyondy and

[2] UCS_i and UCS_d stand for unconfined compressive strength of intact rock and rock with micro-cracks, respectively (see "Appendix" for definition).

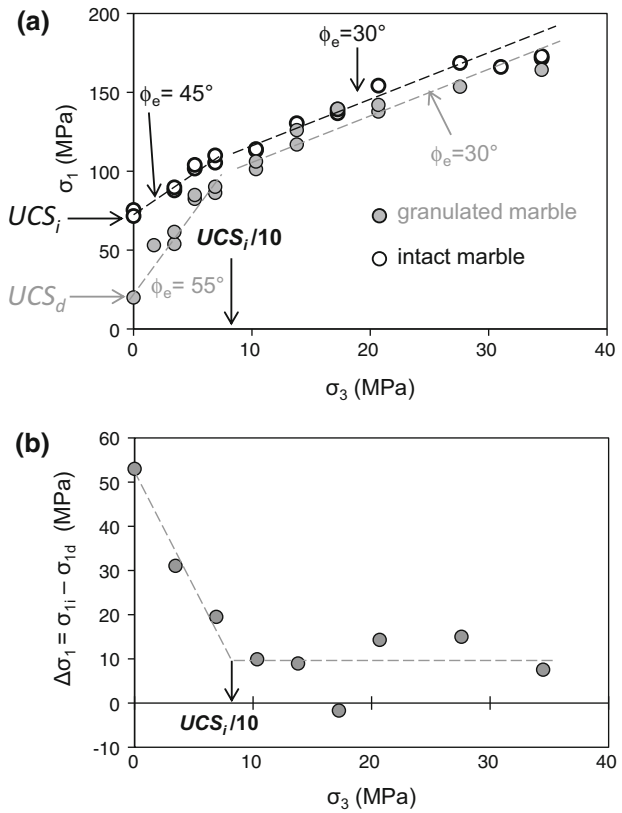

Fig. 1 **a** Unconfined and confined strengths of intact and granulated Wombeyan marble (after Gerogiannopoulos 1976) and calculated equivalent friction angles for confinement ranges less than 10 % of intact *UCS* ($\sigma_3 < UCS_i/10$) and greater than 10 % of intact *UCS* ($\sigma_3 > UCS_i/10$); **b** plot of strength degradation ($\Delta\sigma_1$) of granulated Wombeyan marble as a function of confinement; showing a rapid strength degradation from $\sigma_3 = 0$ MPa to a confinement equal to 10 % of intact *UCS* ($\sigma_3 < UCS_i/10$), and a relatively constant degradation (less than 15 MPa) for confinements greater than 10 % of intact *UCS* ($\sigma_3 > UCS_i/10$)

Cundall 2004), and its grain-based model (*GBM*) developed by Potyondy (2010), to simulate the laboratory behavior of intact and heat-treated Wombeyan marble reported by Gerogiannopoulos (1976). In the *GBM*, a rock specimen is simulated with polygonal, deformable and breakable grains. The grains consist of a number of circular particles (balls) bonded together using parallel bonds, and the grain boundaries are simulated using the smooth-joint contacts. In *PFC2D*, a parallel bond can be envisioned as a set of elastic springs, uniformly distributed over a rectangular cross section lying on the contact plane and centered at the contact point. The smooth-joint contact captures the behavior of an interface regardless of the local particle contact orientation along the interface. When a smooth-joint contact breaks (either in tension or shear), the balls that are located on opposite sides of the smooth-joint plane can overlap to allow particle sliding along the joint plane, rather than forcing the balls to move around each other, which is the case when a parallel bond breaks. Figure 2a shows the *GBM* used by Bahrani et al. (2014) for simulating laboratory tests on intact and heat-treated Womebeyan marble. Axial and lateral pressures in the unconfined and confined tests are applied using walls which are attached to the four sides of the synthetic specimen following the procedure described by Potyondy and Cundall (2004). Figure 2b shows the particles inside the grains and smooth-joint contacts that are used to simulate the grain boundaries, and Fig. 2c illustrates the locations of parallel bonds, which provide the bonds between the particles inside the grains. The calibration results are presented in Fig. 2d.

The main assumptions made by Bahrani et al. (2014) for the calibration of the grain-based models on intact and granulated Wombeyan marble strengths were as follows:

1. Heating intact marble affected the mechanical properties of the grain boundaries, but not the grains. Therefore, components of grains were assigned the same properties in the models of intact and granulated marble.
2. The grain boundaries in the granulated marble have zero tensile strength and cohesion. Therefore, tensile strength and cohesion of the smooth-joint contacts in the model of granulated marble were set to zero.
3. Heating marble had no effect on the frictional properties of the grains and grain boundaries. Therefore, the smooth-joint contacts were assigned the same friction angle in the models of intact and granulated marble.

Table 1 lists the calibration results in terms of micro-properties for the grains (balls and parallel bonds) and Table 2 for the grain boundaries (smooth-joint contacts). The details of the calibration process are described by Bahrani et al. (2014).

3 Shear Strength Degradation of Rock Joint

In a direct shear test on an intact rock specimen, the failure envelope in the high normal stress range can be approximated as a line with a slope equal to the rock basic friction angle ϕ_b and an apparent cohesion c (Fig. 3a). If the same rock contains a smooth joint with zero cohesion (Fig. 3b), the shear strength of the rock joint is represented by a linear envelope and a slope equal to the joint basic friction angle ϕ_j. Assuming that the shear strength envelope is linear,

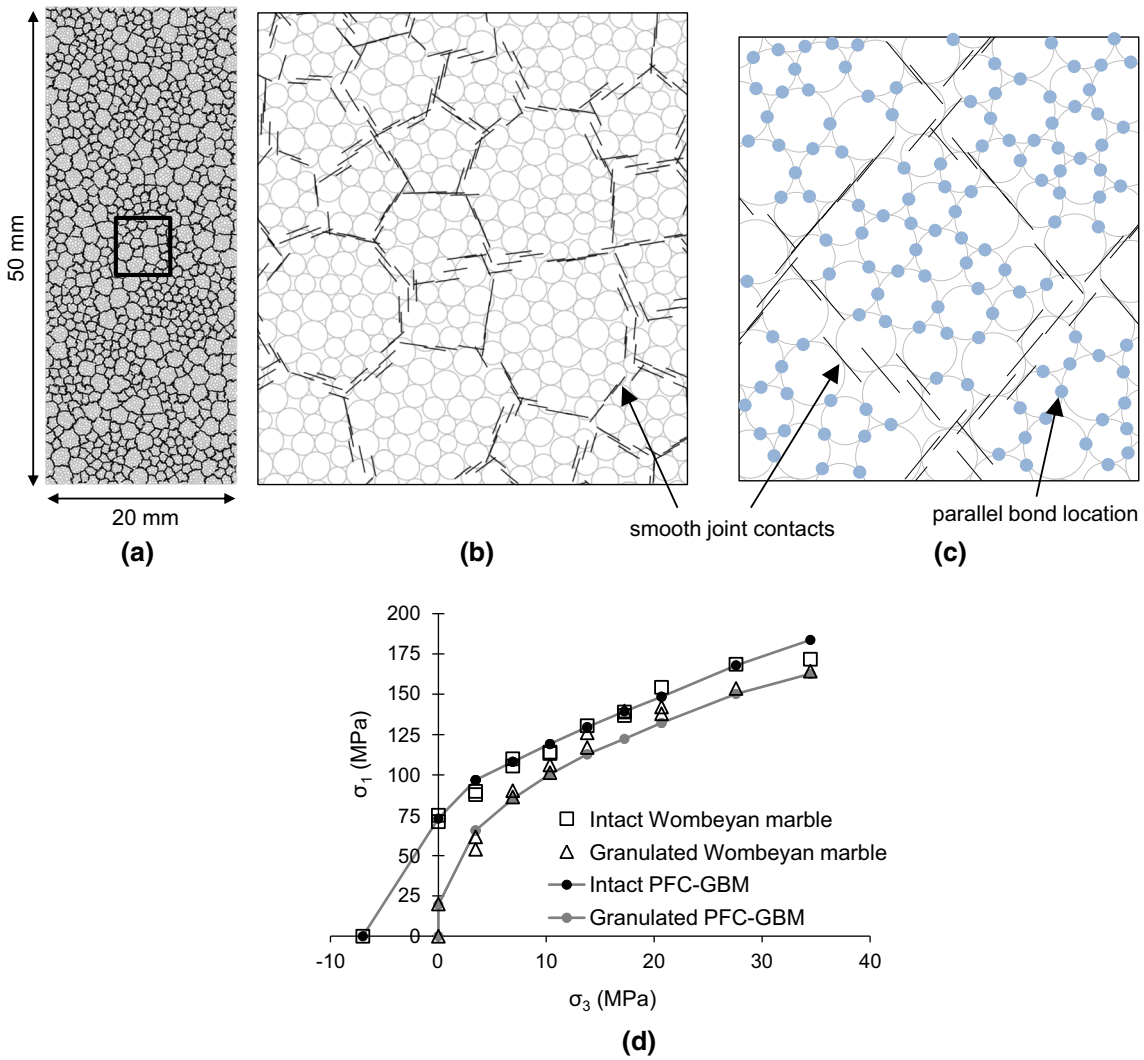

Fig. 2 **a** Grain-based model of Wombeyan marble; **b** larger view of the boxed area in (**a**), showing the grain boundaries simulated using the smooth-joint contacts and grains that consist of a number of circular particles; **c** locations of parallel bonds (shown with *blue circles*), which provide bonds between the particles inside the grains; **d** correspondence between laboratory triaxial test data for intact and granulated Wombeyan marble with numerical simulation results (after Bahrani et al. 2014)

Fig. 3b shows that the reduction in the shear strength of the joint from that of the rock (shear strength degradation: $\Delta\tau = \tau_{\text{rock}} - \tau_{\text{joint}}$) is independent of normal stress (assuming $\phi_b = \phi_j$). For a rough joint with a roughness angle of i, as shown in Fig. 3c, the shear strength of the rock joint can be represented by a bilinear envelope as suggested by Patton (1966). When comparing the shear strength envelopes of intact and jointed rocks, it is evident from Fig. 3c that the shear strength degradation $\Delta\tau$ decreases with increasing normal stress up to a critical normal stress. Beyond this critical normal stress, the shear strength degradation remains constant independent of normal stress.

Considering the rough joint and the intact rock in the rock joint system as an analogue for the grain boundaries and grains, respectively, it is possible to explain the laboratory strength behavior of granulated Wombeyan marble as a function of confinement. As shown in Fig. 1a and discussed by Bahrani et al. (2014), at low confinement up to a confining pressure threshold of about $UCS_i/10$, failure occurs mainly along the grain boundaries. It can be seen in Fig. 1a that for this confinement range ($\sigma_3 \leq UCS_i/10$), the strength envelope of granulated marble is steep and has an equivalent friction angle of 55°. Beyond this confining pressure threshold,

Table 1 Calibrated micro-properties of the grains (balls and parallel bonds) in the grain-based models of intact and granulated Wombeyan marble (Bahrani et al. 2014)

Micro-properties	Intact and granulated
Minimum particle (ball) radius	0.12 mm
Ratio of maximum to minimum ball radius	1.66
Contact normal to shear stiffness ratio	2.5
Parallel bond normal to shear stiffness ratio	2.5
Contact modulus	50 GPa
Parallel bond modulus	50 GPa
Ball friction coefficient	0.5
Parallel bond radius multiplier	1
Parallel bond normal (tensile) strength	110 MPa
Parallel bond cohesion	110 MPa
Parallel bond friction angle	0°

Table 2 Calibrated micro-properties of the grain boundaries (smooth-joint contacts) in the grain-based models of intact and granulated Wombeyan marble (Bahrani et al. 2014)

Micro-properties	Intact	Granulated
Smooth-joint normal to shear stiffness ratio	2.5	2.5
Smooth-joint stiffness factor	0.8	0.2
Smooth-joint normal (tensile) strength	10 MPa	0 MPa
Smooth-joint cohesion	65 MPa	0 MPa
Smooth-joint friction angle	0°	0°
Smooth-joint friction coefficient	1.2	1.2

the sliding along the grain boundaries is inhibited and failure occurs by breaking through the grains.

In the following sections, various densities of cracks in the form of frictional grain boundary cracks are introduced to the calibrated models to investigate their influence on rock strength and to develop an approach to estimate the confined strength of rocks with micro-cracks.

4 Simulation of Crack-Damaged Rock Specimens

As mentioned earlier, the calibration of the *GBM*s was based on the assumption that heating intact marble affected the mechanical properties of the grain boundaries. Thus, the smooth-joint contacts, representing grain boundaries in the model of intact marble were treated as cohesive, and the smooth-joint contacts in the model of granulated marble as frictional. In nature, a rock specimen may consist of a combination of cohesive and frictional grain boundaries. In terms of strength, the intact specimen (without cracks) is stronger than the specimen that contains micro-cracks. It is expected that the strength of crack-damaged rock specimens decreases with increasing the density of cracks.

The crack-damaged rock specimens were simulated by assigning the properties of the frictional grain boundaries (obtained from the grain-based model of granulated marble listed in Table 2) to a specific number of grain boundaries. The properties of the frictional smooth-joint contacts were assigned in increments of 10 %, from 0 to 90 %, to all of the smooth-joint contacts. SJ_f, stands for frictional smooth joints and refers to the percentage of smooth-joint contacts that are in a frictional state in a *GBM*.[3] For example, Fig. 4a shows a grain-based specimen, where 50 % of the smooth-joint contacts are frictional (i.e., $SJ_f = 50$ %) and have the properties of model of granulated marble listed in Table 2. The intact and frictional grain boundaries (smooth-joint contacts) are shown in Fig. 4a with green and black lines, respectively. The grain-based specimens with frictional smooth-joint contacts are essentially homogeneous as the frictional smooth-joint contacts are randomly oriented and located inside the synthetic specimens and therefore do not generate preferential planes of weakness. Therefore, the grain-based specimens with frictional smooth-joint contacts are considered to be representative models of rock specimens with micro-cracks.

The simulation results are presented in Fig. 4b–d. Each point in these graphs represents the average of three values for strength or strength degradation. An example of variability in the strength degradation for the grain-based specimens with crack densities of 10, 50, and 100 % is presented in Sect. 5. The degradation in peak strength and the related changes in stress–strain characteristics as well as changes in failure mode are discussed in the following sections.

4.1 Peak Strength

Three *GBM*s with different grain structure and particle arrangement realizations were built for each grain-based specimen with various crack densities, and uniaxial and triaxial compression tests were conducted.

Figure 4b shows the unconfined and confined strengths of the grain-based specimens with the percentage of frictional smooth-joint contacts ranging from 0 % (i.e., model of intact marble) to 100 % (i.e., model of granulated marble) in the σ_1 versus σ_3 stress space. The plots of the

[3] $SJ_f = 0$ % refers to a grain-based specimen where all the smooth-joint contacts are cohesive, and $SJ_f = 100$ % refers to a grain-based specimen where all the smooth-joint contacts are frictional.

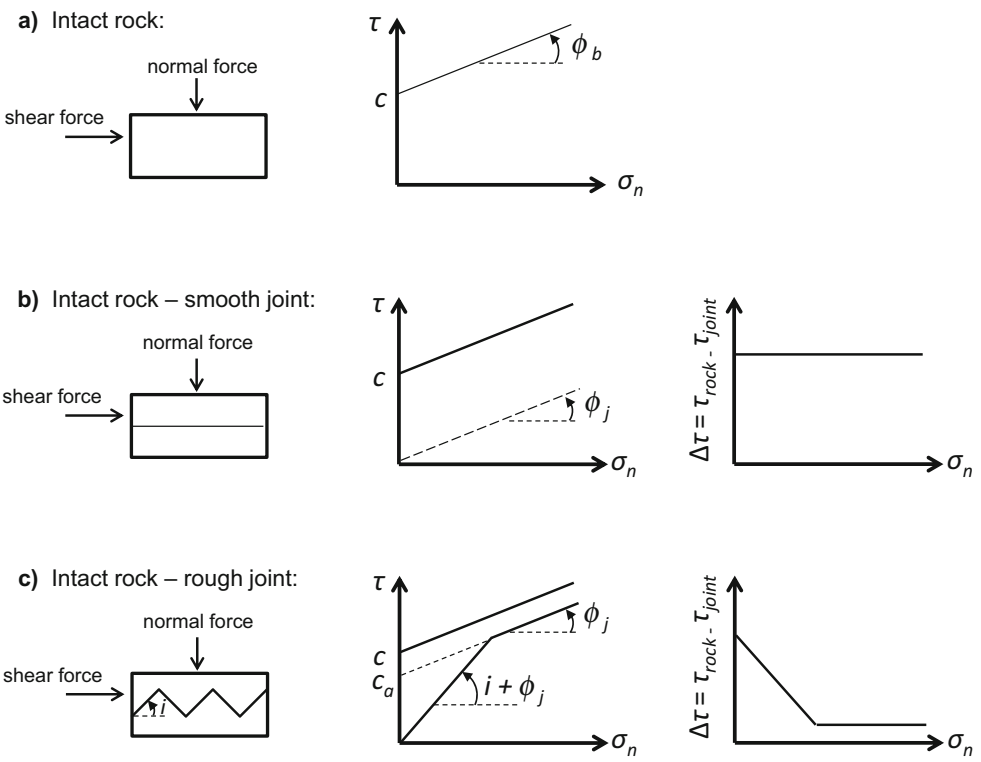

Fig. 3 **a** Shear strength of intact rock as a function of normal stress. Shear strength and shear strength degradation ($\Delta\tau$) of: **b** a smooth joint; and **c** a rough joint with a roughness angle of i, as a function of normal stress, assuming $\phi_b = \phi_j$

strength degradation ($\Delta\sigma_1$) as a function of confinement in Fig. 4c suggest that the strength degradation of grain-based specimens with micro-cracks decreases with increasing confinement up to the confining pressure of about $UCS_i/10 = 7$ MPa and remains more or less constant at higher confinements with strength degradations ranging from less than 5 MPa to about 20 MPa, beyond the confining pressure of 7 MPa. Figure 4d shows the equivalent friction angles calculated for the low ($\sigma_3 < UCS_i/10$) and high ($\sigma_3 > UCS_i/10$) confinement portions of the strength envelopes as a function of crack density. The equivalent friction angle at low confinement increases with increasing crack density, whereas it is independent of crack density at high confinement.

4.2 Stress–Strain Response

The stress–strain curves are presented in Fig. 5 for crack densities of 0, 20, 50, 80 and 100 % and for confining pressures of 0 MPa (Fig. 5a), 6.9 MPa (Fig. 5b), and 34.5 MPa (Fig. 5c). At zero confinement, both the strength and the deformation modulus decrease with increasing crack density (Fig. 5a). The axial strain at peak strength is insensitive to the crack density, but the initial post-peak response becomes more ductile with increasing crack density. This is due to the increase in the number of frictional grain boundaries.

The stress–strain curves of the grain-based specimens at confining pressures of 6.9 and 34.5 MPa, presented in Fig. 5b, c, show that the grain-based specimens with micro-cracks become more ductile with increasing crack density and confinement. The axial strain at peak strength increases with increasing crack density. The influence of micro-cracks becomes less significant in terms of peak strength reduction at high confinement.

4.3 Failure Mode

The failure modes including the location and orientation all the grain-scale micro-cracks (inter- and intra-grain) generated during loading of the grain-based specimens with initial crack densities of $SJ_f = 0$, 50 and 100 % at confining pressures of 0, 6.9 and 34.5 MPa are shown in Fig. 6. Note that the initial micro-cracks are purely frictional since they are in a broken state from the start of the test and therefore cannot be seen in these figures. For this reason, no inter-grain micro-cracks can be seen in the grain-based specimen in which all the smooth-joint contact are frictional (i.e., $SJ_f = 100$ %). Close-up views of the boxed areas in Fig. 6 are presented in Fig. 7.

The typical transition in the failure mode for brittle rocks from axial splitting at low confinement to shear failure at high confinement is observed in all grain-based specimens with various cracks densities. As shown in Fig. 6, failure at zero confinement is dominated by subvertical cracks. A number of these micro-cracks connect to generate relatively long macroscopic subvertical fractures

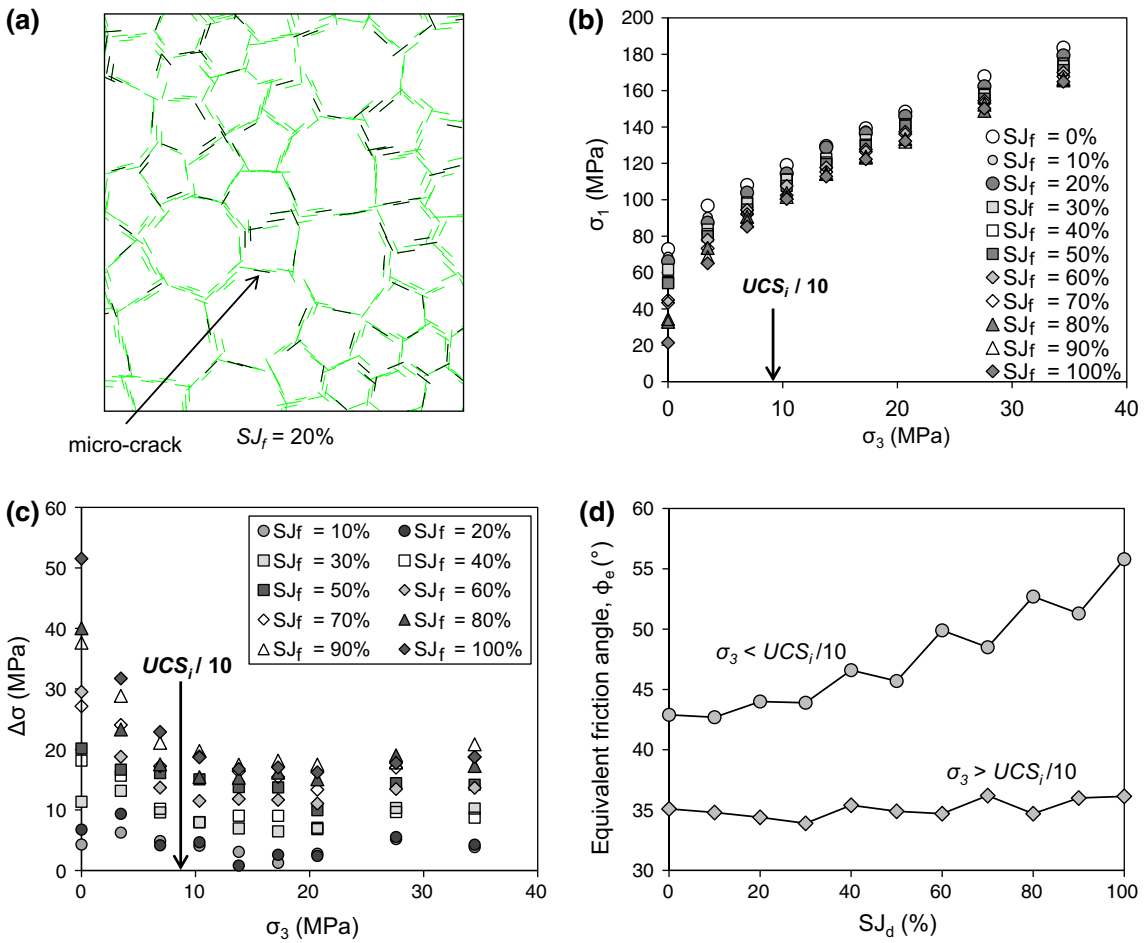

Fig. 4 **a** A grain-based specimen where 50 % of the smooth-joint contacts are frictional ($SJ_f = 50$ %). *Green* and *black* grain boundaries refer to cohesive and frictional smooth-joint contacts; **b** unconfined and confined strengths of grain-based specimens with various densities of frictional smooth-joint contacts representing micro-cracks; **c** strength degradation ($\Delta\sigma_1$) of grain-based specimens with micro-cracks as a function of confinement; **d** influence of micro-crack density on the equivalent friction angle of grain-based specimens at low ($\sigma_3 < UCS_i/10$) and high ($\sigma_3 > UCS_i/10$) confinements

(e.g., see the micro-cracks in the boxed area of Fig. 6a and the corresponding images in Fig. 7). Close to the boundaries of the specimens, clusters of micro-cracks generate macroscopic shear fractures (see arrows in Fig. 6a, d).

At the confining pressure of 6.9 MPa, the failure modes of the grain-based specimens with the crack densities of $SJ_f = 0$ and 50 % are similar (Fig. 6b, e). In the grain-based specimen in which all the smooth-joint contacts are frictional (i.e., $SJ_f = 100$ %), two inclined fracture zones (shear bands) consisting of a number of intra-grain cracks can be identified (see arrows in Fig. 6h). The corresponding images in Fig. 7 illustrate the details of these fracture zones in terms of the types of micro-cracks and their particle velocity vectors.

At the confining pressure of 34.5 MPa, the failure modes of the grain-based specimens with varying crack densities are similar (Fig. 6c, f, i). The failure is dominated by two or more macroscopic and conjugate shear fractures (e.g., arrows in Fig. 6i point to some of these shear fractures). The macroscopic shear zones appear to be the result of interaction between intra-grain tensile and shear cracks.

Particle velocity vectors along with the types of micro-cracks (upper figures) and grain boundaries (lower figures) are shown in Fig. 7 to emphasize the failure modes at the grain scale. Three main modes of failure can be distinguished from the velocity vectors; opening, shearing, and combined opening-shearing. In the opening mode, the directions of velocity vectors are opposite, and they are nearly perpendicular to the direction of applied load (e.g., $SJ_f = 0$ % and $\sigma_3 = 0$ MPa in Fig. 7). Shearing occurs when the direction of velocity vectors of two groups of particles is opposite, and the resulting shear fracture is inclined relative to the direction of applied load (e.g., $SJ_f = 0$ % and $\sigma_3 = 34.5$ MPa in Fig. 7). Combined

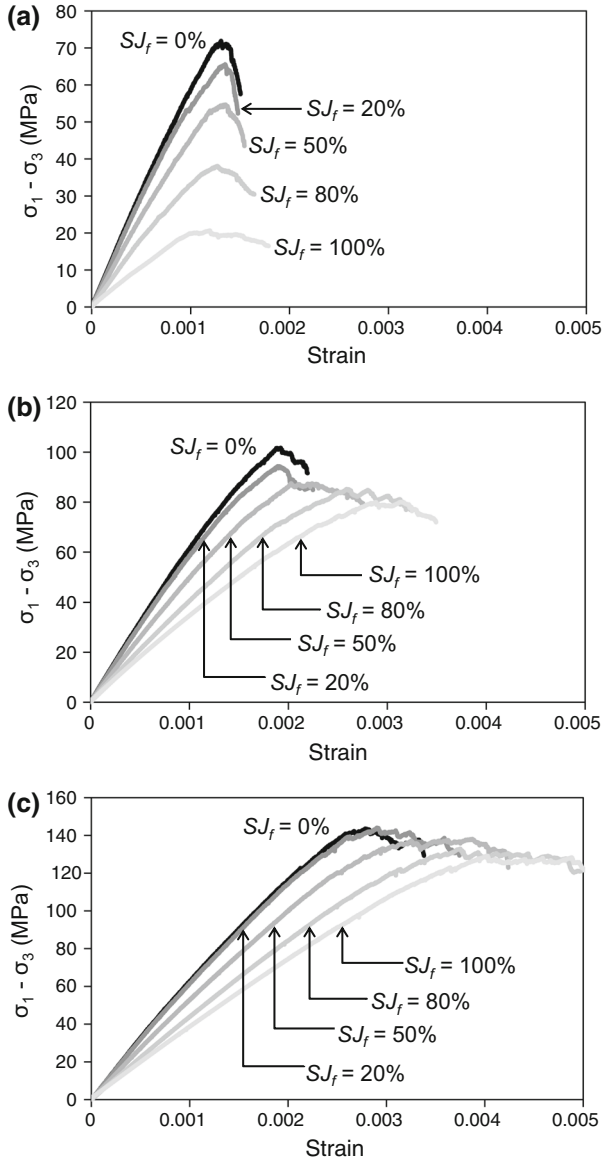

Fig. 5 Stress–strain curves of grain-based specimens with various micro-crack densities at: **a** $\sigma_3 = 0$ MPa, **b** $\sigma_3 = 6.9$ MPa, and **c** $\sigma_3 = 34.5$ MPa

opening-shearing contains components of these two failure modes (e.g., $SJ_f = 0$ % and $\sigma_3 = 6.9$ MPa in Fig. 7).

At zero confinement, the failure mode at the grain scale mainly consists of a combination of opening and combined opening-shearing, with opening being the dominant failure mode. Opening or extension failure, as shown in Fig. 7, occurs mainly along the nearly vertical grain boundaries. At a confining pressure of 6.9 MPa, a combination of the three modes can be seen. The combined opening-shearing can occur along the grain boundaries or through the grains. The main mode of failure at the confining pressure of 34.5 MPa is shearing, which occurs by failing through the grains. Failure modes described above were also observed in the other grain-based specimens with micro-cracks.

In the following section, these modeling results are used to develop a semi-empirical approach for the estimation of the confined strength of rocks with micro-cracks.

5 Strength Degradation Approach (SDA)

Bahrani and Kaiser (2013) defined a degradation parameter (DP_d), based on laboratory test results on intact and damaged rocks as follows:

$$DP_d = (\Delta\sigma_1/\sigma_{1i}) \times 100 = [(\sigma_{1i} - \sigma_{1d})/\sigma_{1i}] \times 100 \qquad (1)$$

where DP_d determines the reduction in the strength of a crack-damaged rock (σ_{1d}) from that of intact rock ($\Delta\sigma_1 = \sigma_{1i} - \sigma_{1d}$) as a percentage of intact rock strength (σ_{1i}).

The DP_d of the grain-based specimens with various crack densities were calculated and plotted in Fig. 8a as a function of confinement normalized to the unconfined compressive strength of intact grain-based specimens (σ_3/UCS_i). In this figure, the DP_d ranges from 5 to 70 % at zero confinement, rapidly decreases to below 20 % at a confining pressure equal to $UCS_i/10$ and remains below 15 % beyond this limit (i.e., for $\sigma_3 > UCS_i/10$). This trend is consistent with the results obtained by Bahrani and Kaiser (2013) who investigated the strength degradation of rock specimens consisting of strength dominating features such as micro-cracks or fractures from their intact strengths as a function of confinement. Note that the data points in Fig. 8a were determined by first averaging the strengths of grain-based specimens (three data points for each confining pressure as shown in Fig. 8b–d as an example for the grain-based specimens with crack densities of $SJ_f = 10$, 50, and 100 %) at different magnitudes of confining pressure and then calculating the DP_d using Eq. 1.

5.1 Determination of Degradation Parameters for Crack-Damaged Rocks

The results of numerical simulations presented in Fig. 8a were used to develop a series of semi-empirical equations to estimate the confined strength of crack-damaged rocks. This approach, which is based on determining the strength degradation of rock containing micro-cracks compared to intact rock, is referred to as the strength degradation approach (*SDA*) throughout this article. The *SDA* provides a means for estimating the confined strength of a crack-damaged rock in a situation where the unconfined and confined

strengths of the intact rock as well as the unconfined strength of the rock containing micro-cracks are known.

An exponential function was used to fit to the results of numerical simulations presented in Fig. 8a. The general form of this function is shown in Fig. 9 and expressed as:

$$y = Ae^{Bx} + E \tag{2}$$

where the values of A and E define the limits of the trendline on the vertical axis, and the value of B defines curvature of the trendline.

A series of least-square regression analyses were conducted to determine the fitting parameters described above. The following three steps were taken to develop the *SDA*.

Step 1 The DP_d values of the grain-based specimens with the crack densities ranging from $SJ_f = 10$–100 % were first plotted against σ_3. The negative exponential function used to fit the data is expressed as:

$$DP_d = (Du_d - Dc_d)e^{[100(-\sigma_3/\sigma_{ci})/c_d]} + Dc_d \tag{3}$$

where Du_d (unconfined degradation) is the value of DP_d at zero confinement, Dc_d (confined degradation) is the value of DP_d at high confinement ($\sigma_3 > UCS_i/10$) where DP_d becomes independent of confining pressure, and c_d controls the curvature of the trend line. An example of this procedure is shown in Fig. 8b–d for the grain-based specimens with the crack densities of $SJ_f = 10$ %, $SJ_f = 50$ %. And $SJ_f = 100$ %. The fitting parameters Du_d, Dc_d and c_d for the grain-based specimens with micro-cracks, which were obtained from the least-square regression analysis are listed in Table 3. The coefficients of determination (R^2) are high (>0.8) for most cases. Poorer fits are obtained for low SJ_f percentages, i.e., $SJ_f < 30$ %. The increase in the coefficient of determination with increasing crack density is interpreted as being related to the change in the failure mechanism at the grain scale. At low SJ_f percentages, a combination of grain and grain boundary cracks drives the specimens to failure. This results in a higher variability in their strength magnitudes (and therefore their strength degradations) than specimens with high SJ_f percentages, where opening and shearing along frictional grain boundaries are the main cause of failure.

The ±95 % confidence intervals (*CI*) as plotted in Fig. 8b–d are indicators of data scatter. The *CI* gives an estimate of an interval within which the mean is expected to occur for a given set of data.

Step 2 As mentioned earlier, the unconfined compressive strengths of intact and crack-damaged rocks and the confined strength of intact rock are the assumed known parameters for the estimation of confined strength of crack-damaged rocks in the *SDA*. Therefore, Du_d (i.e., DP_d value at zero confinement) can be directly determined from laboratory test data according to the following equation:

$$Du_d = [(\sigma_{ci} - UCS_d)/\sigma_{ci}] \times 100 \tag{4}$$

where σ_{ci} is the uniaxial compressive strength of the intact rock obtained by back projecting the Hoek–Brown failure criterion fitted to the triaxial test data of intact rock to the unconfined state (according to the procedure described by Hoek and Brown 1997) and UCS_d is the average unconfined compressive strength of crack-damaged specimens directly obtained from unconfined compression tests (the difference between σ_{ci} and *UCS* is explained in more detail in the "Appendix").

Step 3 Du_d is in fact a measure of the level of damage (crack density) in a specimen; the higher the crack density in a specimen, the higher the Du_d value. The parameters Dc_d and c_d are unknown parameters in this approach. Therefore, equations that relate these two parameters to Du_d had to be developed. For this purpose, the values of c_d and Dc_d were plotted against Du_d in Fig. 10a, b. These figures indicate that Dc_d increases nonlinearly with increasing Du_d. The rate of increase in Dc_d gradually decreases, especially for Du_d values greater than 50 %. Figure 10b shows that the curvature parameter c_d decreases rapidly as Du_d increases and tends to level off for $Du_d > 50$ %.

In Fig. 10a, the exponential function was forced to pass through the origin as the strength degradation in a specimen with no micro-crack is zero. Therefore, A and E in the general exponential function (Eq. 2: $y = Ae^{Bx} + E$) had to be equal in magnitude. The confined degradation Dc was determined to be in the form of:

$$Dc_d = -17.3e^{-0.017Du_d} + 17.3 \tag{5}$$

In determining the equation for the curvature parameter c_d (Fig. 10b), no constraint was used to

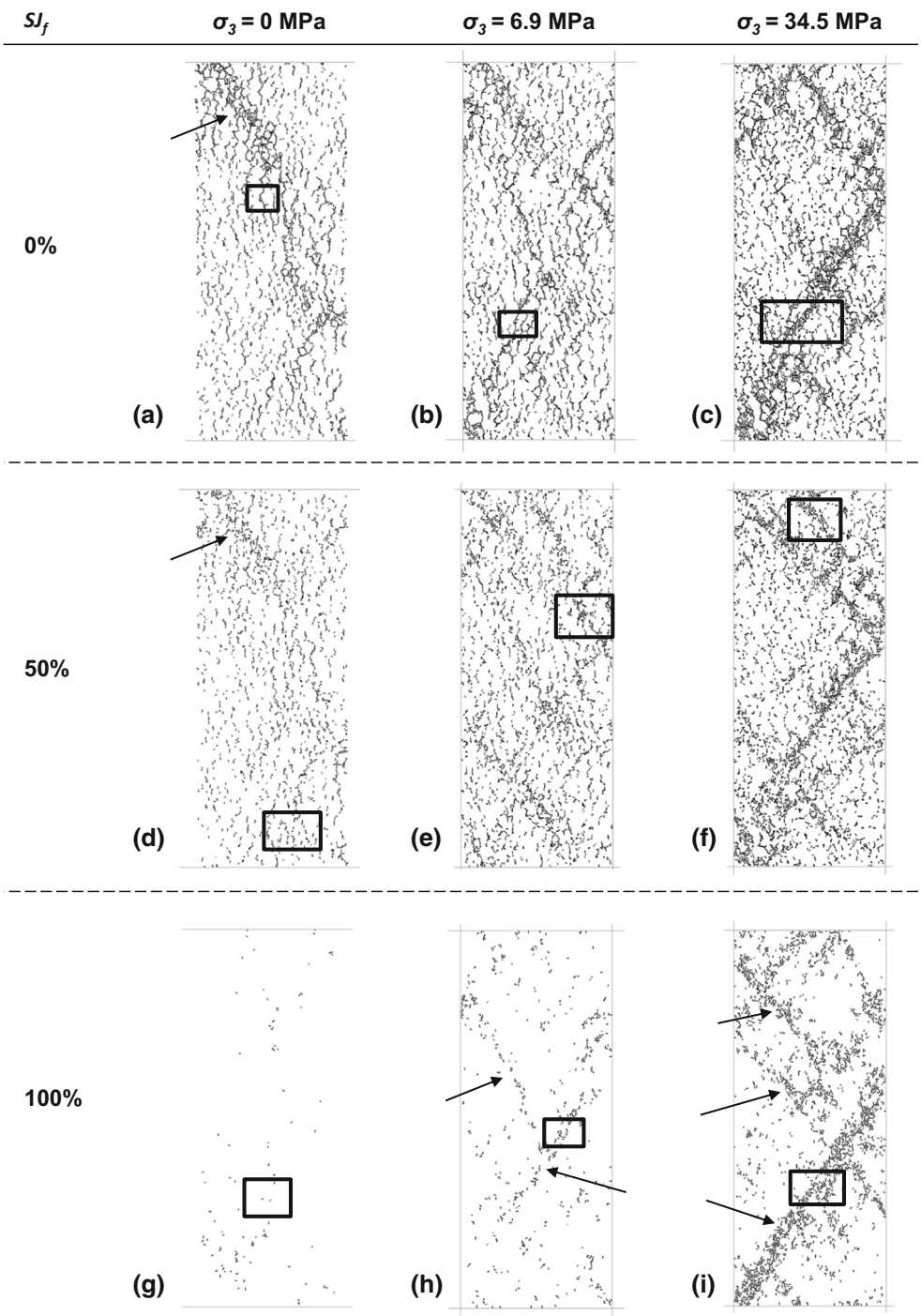

Fig. 6 Failure modes of grain-based specimens with micro-crack densities of 0, 50, and 100 %, at 0, 6.9 and 34.5 MPa confining pressures. The *boxed areas* are zoomed in and shown in Fig. 7

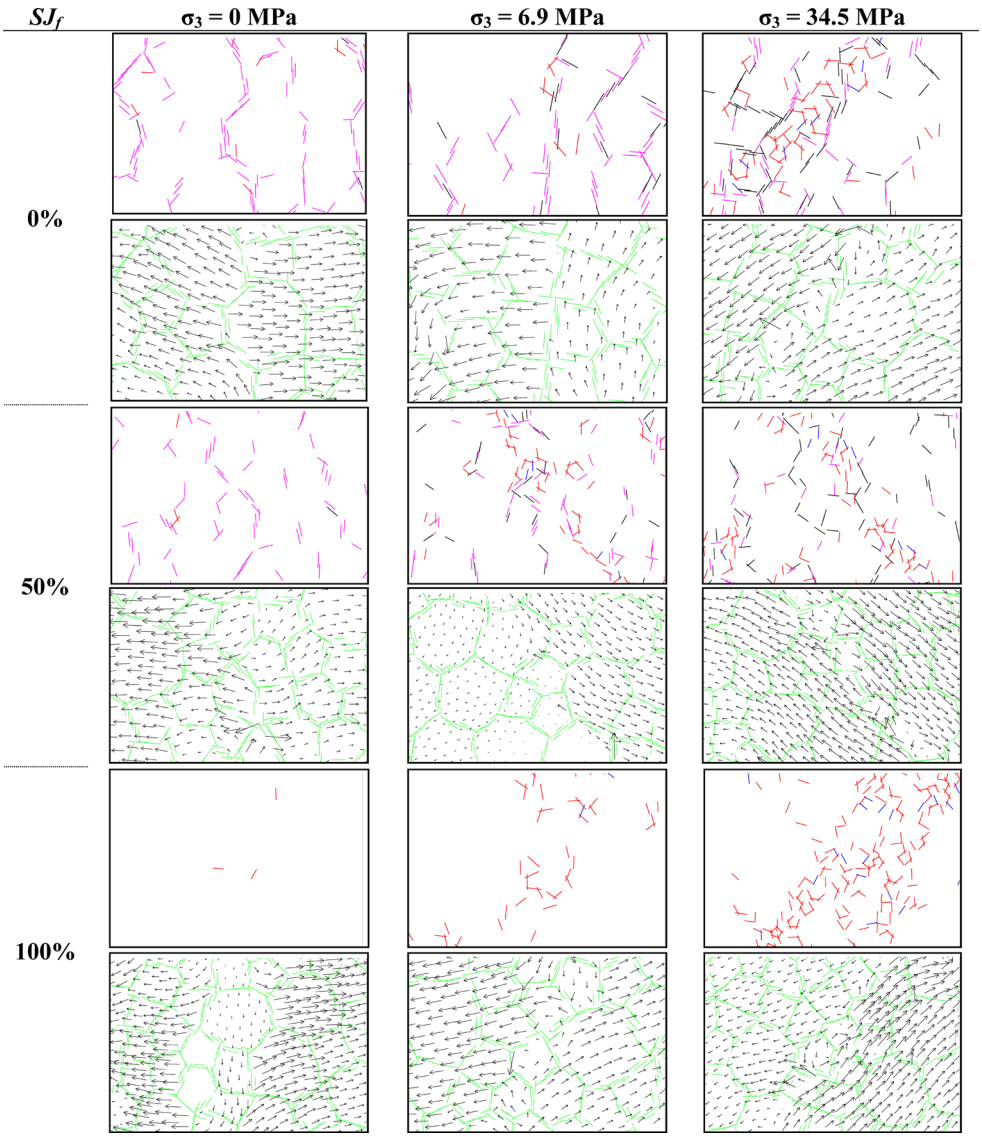

Fig. 7 Grain-scale failure modes of grain-based specimens with micro-crack densities of 0, 50, and 100 %, at 0, 6.9 and 34.5 MPa confining pressures. *Green* refers to intact grain boundaries, *magenta* and *black* refer to inter-grain tensile and shear cracks, respectively, and *red* and *blue* refer to intra-grain tensile and shear cracks, respectively. For locations of micro-cracks see the *boxed areas* in Fig. 6

define the fitting parameters. The curvature parameter c_d was found to be related to Du_d according to:

$$c_d = 10.8e^{-0.055Du_d} + 4.5 \quad (6)$$

The least-square regression analyses resulted in satisfactory coefficients of determination of $R^2 = 0.93$ and 0.82 for Dc_d and c_d, respectively. The ± 95 % *CI* curves are also plotted in Fig. 10a, b. It is suggested that since there is only one data point for Du_d greater than 70 %, Eqs. 5 and 6 should be used with care when dealing with rocks with high Du_d values ($Du > 70$ %). Note that this point corresponds to the grain-based specimen with the crack density of $SJ_f = 100$ %.

5.2 Estimation of the Confined Strength of Crack-Damaged Rocks Using the SDA

Now that the strength degradation of rock specimens with micro-cracks can be estimated as a function of confinement, the confined strength of such specimens can be estimated after rearranging Eq. 1 in the form of:

$$\sigma_{1d} = \sigma_{1i} \times [1 - (DP_d/100)] \quad (7)$$

The following steps provide an estimate of the confined strength of rocks containing micro-cracks using the *SDA*:

Step 1 The Hoek–Brown (*HB*) failure envelope is fitted through the unconfined and confined strengths of intact rock following the procedure explained by Hoek and Brown (1997)

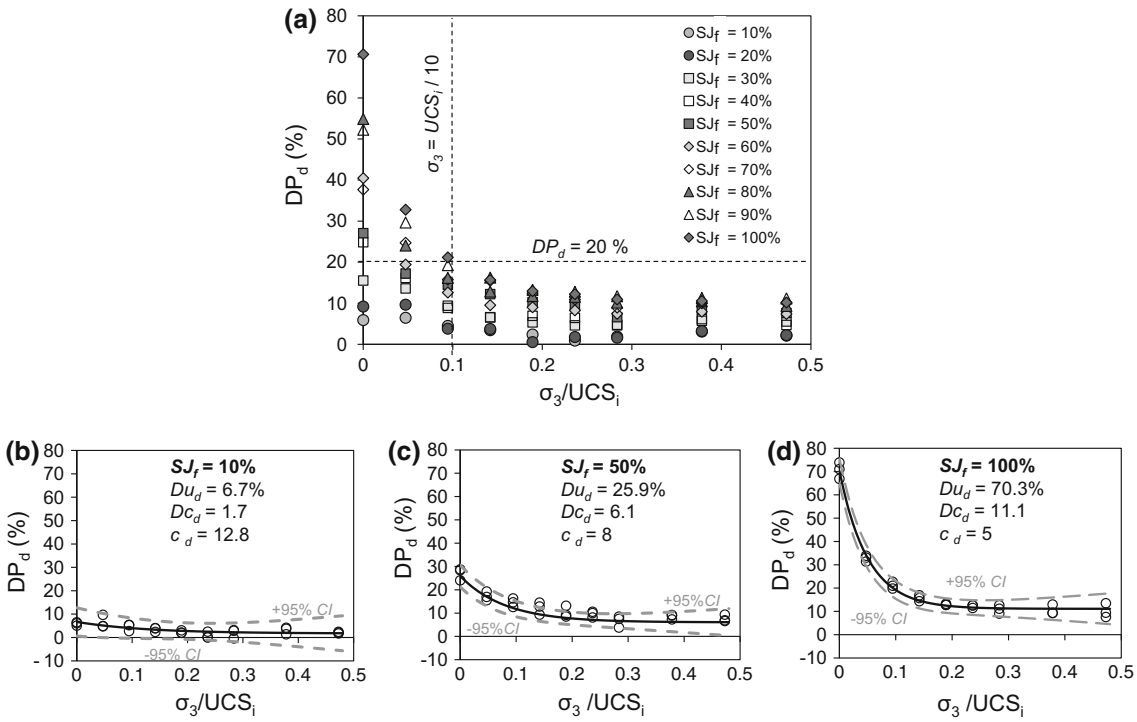

Fig. 8 **a** Strength degradation graph for grain-based specimens with micro-crack densities ranging from $SJ_f = 10$ % to $SJ_f = 100$ %); strength degradation graph and fitting parameters Du_d, Dc_d, and c_d for the grain-based specimens with micro-crack densities of: **b** $SJ_f = 10$ %; **c** $SJ_f = 50$ %; **d** $SJ_f = 100$ %. ±95 % confidence intervals are shown with *dashed gray curves* in (**b**) to (**d**)

Step 2 Du_d is determined from the unconfined compressive strength of intact rock (σ_{ci}) obtained from triaxial compression tests and the average unconfined strength of rocks with micro-cracks (UCS_d) using Eq. 4

Step 3 The values of Dc_d, c_d, and DP_d are determined from Eqs. 5, 6, and 3, respectively

Step 4 The confined strength of crack-damaged rocks is then estimated using Eq. 7

This approach is illustrated and examined on the following case examples.

6 Case Studies

In the following, the applicability of the *SDA* for estimating the confined strength of rocks with micro-cracks is first investigated using the results of laboratory tests on rocks containing micro-cracks. The crack-damaged rock specimens include granulated Wombeyan marble (Rosengren and Jaeger 1968; Gerogiannopoulos 1976), granulated Carrara marble (Gerogiannopoulos 1976), and damaged Lac du Bonnet granite (Martin 1993).

6.1 Granulated Wombeyan and Carrara Marble

Rosengren and Jaeger (1968) and Gerogiannopoulos (1976) conducted laboratory tests on coarse-grained Wombeyan and fine-grained Carrara marble. The intact marble specimens were heated up to 600 °C, and the anisotropy of thermal expansion of calcite grains caused the separation of grains at their boundaries. The results of laboratory tests on Wombeyan marble by Gerogiannopoulos (1976) (Fig. 11a) and Rosengren and Jaeger (1968) (Fig. 11b) and Carrara marble by Gerogiannopoulos (1976) (Fig. 11c) demonstrate a similar trend in terms of rapid increase in the strength of granulated marble with increasing confinement. As can be seen from Fig. 11a, the *SDA* predicts this rapid increase in the strength of granulated marble up to a critical confining pressure with a value of about $UCS_i/10$ (i.e., 7.0 MPa); however, it tends to underestimate the confined strength beyond this limit.

Figure 11b, c show the results of laboratory tests on Wombeyan and Carrara marble reported by Rosengren and Jaeger (1968) and Gerogiannopoulos (1976), respectively, and their strength envelopes estimated by the *SDA*. It can be seen that the *SDA* captures the rapid increase in the strengths of granulated Wombeyan and Carrara marble at low confinement and, considering the inherent variability

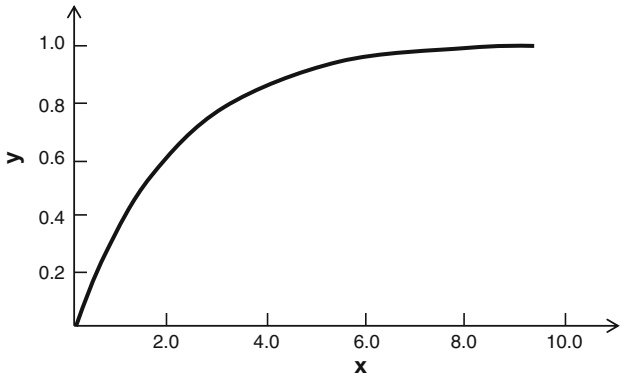

Fig. 9 An example of exponential function that follows the general function (Eq. 2) with A = −1, B = −0.5 and E = 1

Table 3 Degradation parameters and coefficient of determination obtained from the least-square regression analysis

SJ_f (%)	Du_d (%)	Dc_d (%)	c_d	R_2
10	6.7	1.7	12.8	0.52
20	10.3	1.6	9.2	0.32
30	16.4	4.7	9.1	0.72
40	25.1	5.1	6.9	0.87
50	25.9	6.1	8.0	0.91
60	40.4	7.9	4.7	0.88
70	37.6	9.7	6.7	0.98
80	54.7	10.8	4.1	0.97
90	52.1	11.3	5.5	0.98
100	70.3	11.1	5.0	0.99

in the strength data, reasonably predicts their confined strengths at high confinement. This is more evident in the case of Wombeyan marble (Fig. 11b).

6.2 Damaged Lac du Bonnet Granite

The Lac du Bonnet (*LdB*) granite cores drilled from the 420 levels of the Underground Research Laboratory (*URL*) in Manitoba, Canada, contained micro-cracks generated during the process of core drilling due to high stress concentrations near the drill bits. Martin and Stimpson (1994) and Eberhardt et al. (1999) suggested that damaged specimens (i.e., those containing micro-cracks) could be identified from the change in the material response when subjected to uniaxial compression; undamaged (intact) specimens from shallow depth responded in a linear elastic manner, whereas damaged specimens from deeper levels initially exhibited a strongly nonlinear response due to micro-crack closure. The unconfined compressive strength of the intact and damaged specimens are 213 ± 20 and 157 ± 18 MPa (mean ± 1 standard deviation), respectively. Figure 12 shows the laboratory test results on intact and damaged specimens of *LdB* granite, along with the strength envelope from the *SDA*, which demonstrates that this approach provides a reasonable fit to the strength of damaged *LdB* granite for the entire range of confinement (i.e., up to 60 MPa confining pressure).

6.3 Assessment of Prediction Quality of SDA

The confidence interval (*CI*) is used in this section to assess the prediction quality of the *SDA*. It is highly unlikely that a best estimate for a parameter from a sample (in this case mean confined peak strength estimated by the *SDA*) be equal to the true (unknown) mean population value. Therefore, it is appropriate to determine an interval, within which one would expect to find the value of the mean. Such intervals are known as confidence intervals (*CI*s). *CI*s should strictly be interpreted with respect to a hypothetical sequence of similar repeated inferences. For example, a 95 % *CI* for the mean indicates that in a long-run of similar experiments and inferences, 95 % of the computed intervals will contain the true (unknown) mean population value and thus, gives 95 % confidence. It is important to emphasize that a 95 % *CI* for the mean does not advocate that the true mean falls in the interval with a probability of 0.95. On the other hand, predilection intervals (*PI*s) deal with future observations of the random variable in question. In other words, *PI*s provide a range with a

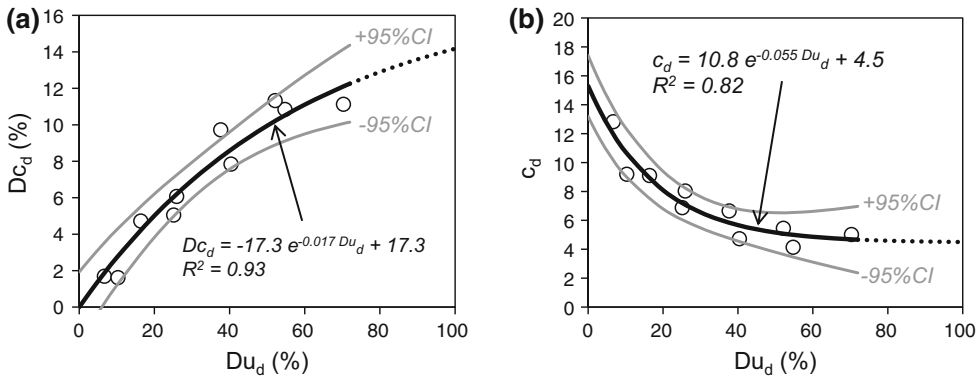

Fig. 10 Relationships between: **a** Dc_d and Du_d; and **b** c_d and Du_d. The ±95 % *CI*s are shown with *gray curves*

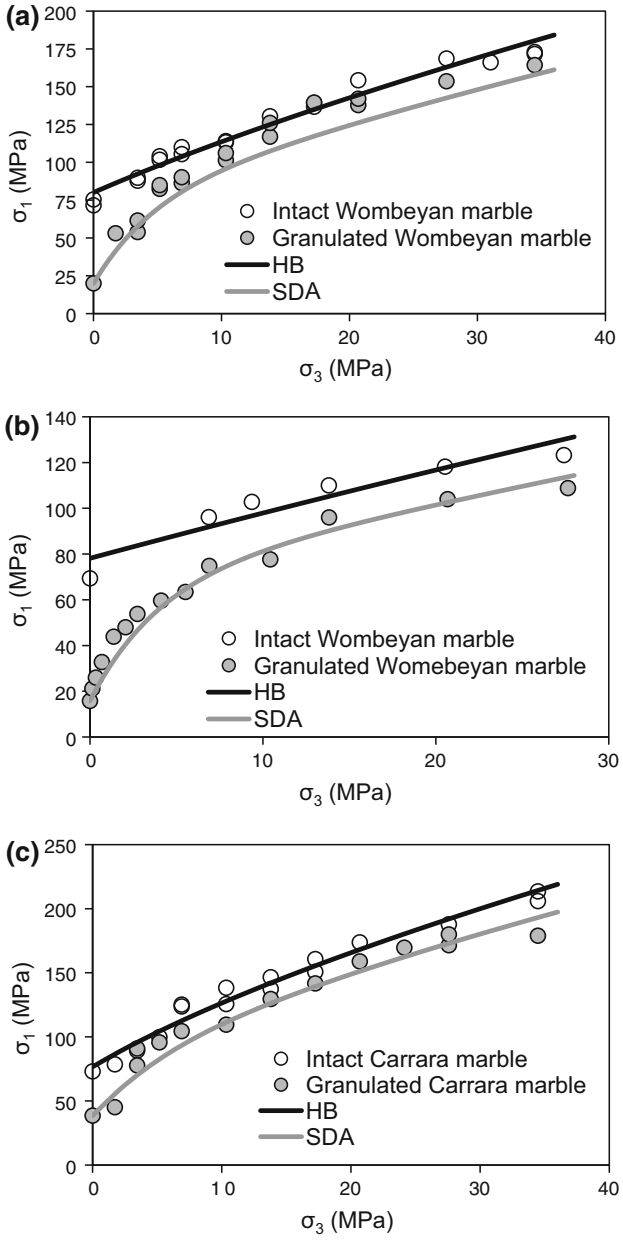

Fig. 11 Laboratory data of intact and granulated: **a** Wombeyan marble tested by Gerogiannopoulos (1976); **b** Wombeyan marble tested by Rosengren and Jaeger (1968); **c** Carrara marble tested by Gerogiannopoulos (1976). The Hoek–Brown (*HB*) failure criterion fitted to the strength of intact rock is shown with *solid black curve*

specified probability (e.g., 0.95) of containing a future observation. For more details on the concepts of *CI*s and *PI*s, see any classical statistics text books.

Since the *SDA* is expected to provide the best estimate of the mean value of the confined peak strength of crack-damaged rocks, the concept of confidence interval (as opposed to the future interval) was used to evaluate the prediction quality of the *SDA*.

The following steps were undertaken to evaluate the prediction quality of the *SDA* approach:

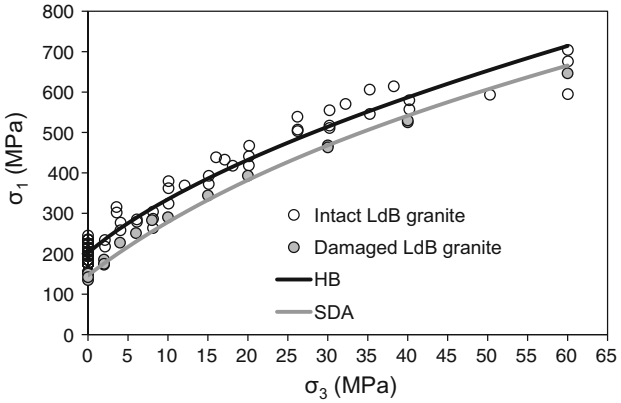

Fig. 12 Laboratory data on intact and damaged *LdB* granite and the strength envelope predicted by the *SDA*. The Hoek–Brown (*HB*) failure criterion fitted to the strength of intact rock is shown with *solid black curve*

Step 1 A nonlinear curve was fitted (using the least-square regression analysis) to the unconfined and confined strengths of the specimens with micro-cracks reviewed in the previous section

Step 2 The ±95 % *CI*s for the nonlinear curve were computed

Step 3 The strength envelopes estimated using the *SDA* were checked against the ±95 % *CI*s

Step 4 Following the definition of confidence interval described above, the confined strength of rocks with micro-cracks estimated using the *SDA* is confirmed if the estimated failure envelope falls between the ±95 % *CI*s

Figure 13 presents the analysis for the case of granulated Wombeyan marble (Gerogiannopoulos 1976). Figure 13a shows the nonlinear curve fitted to the triaxial data. Figure 13b demonstrates that the estimated strength envelope based on the *SDA* follows the −95 % *CI* calculated for the nonlinear curve fitted to the triaxial test results of granulated Wombeyan marble.

Similar analyses were conducted for the case of granulated Wombeyan marble reported by Rosengren and Jaeger (1968), as presented in Fig. 14. Figure 14a shows the nonlinear curve fitted to the triaxial test data as well as the ±95 % *CI*s. Figure 14b shows that the strength envelope based on the *SDA* falls between the ±95 % *CI*s.

The results of analyses for Carrara marble (Gerogiannopoulos 1976) and *LdB* granite (Martin 1993) are presented in Fig. 15a–d. As can be seen in Fig. 15b, d, the strength envelopes estimated using the *SDA* fall between the ±95 % CIs calculated for the nonlinear curve fitted to the triaxial data presented in Fig. 15a, c.

The confidence interval is a useful method when trying to constrain a data set and provide upper and lower bounds. Such intervals can be used for

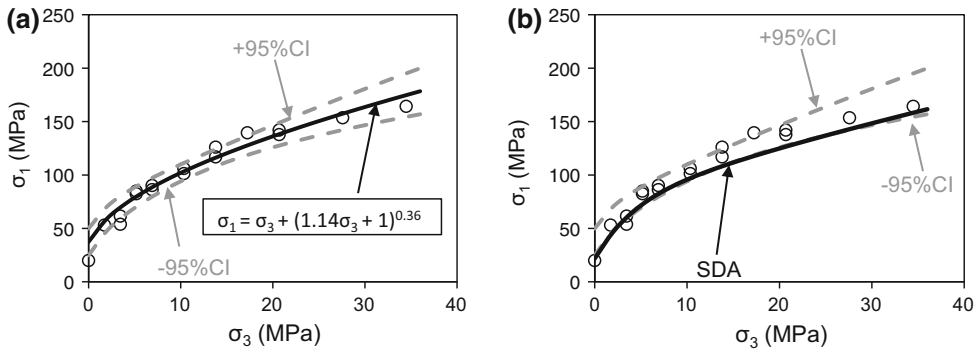

Fig. 13 Assessment of prediction quality of the *SDA* for the estimation of confined strength of granulated Wombeyan marble reported by Gerogiannopoulos (1976): **a** the nonlinear curve fitted to the triaxial test data and the calculated ±95 % confidence intervals; **b** strength envelope estimated using the *SDA* and comparison with the ±95 % confidence intervals

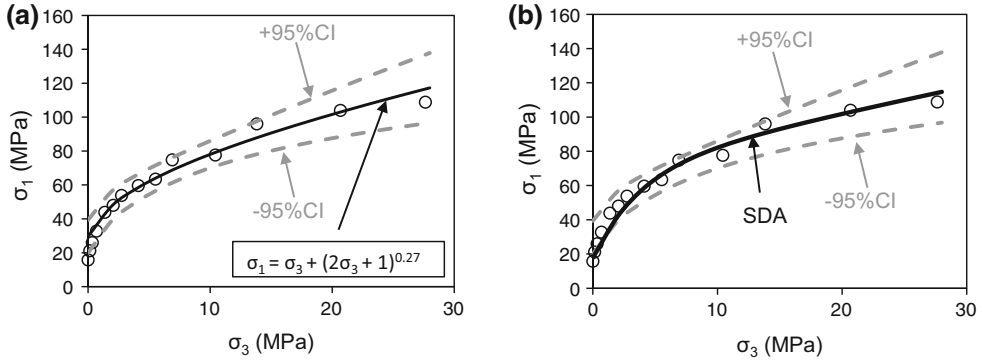

Fig. 14 Assessment of prediction quality of the *SDA* for the estimation of confined strength of granulated Wombeyan marble reported by Rosengren and Jaeger (1968): **a** the nonlinear curve fitted to the triaxial test data and the calculated ±95 % confidence intervals; **b** strength envelope estimated using the *SDA* and comparison with the ±95 % confidence intervals

Fig. 15 Assessment of prediction quality of the *SDA* for the estimation of confined strengths of: **a**, **b** granulated Carrara marble reported by Rosengren and Jaeger (1968); and **c**, **d** *LdB* granite reported by Martin (1993). **a**, **c** The nonlinear curve fitted to the triaxial data and the ±95 % confidence intervals calculated for granulated marble and damaged *LdB* granite, respectively, and **b**, **d** the strength envelopes estimated using the *SDA* for granulated marble and damaged *LdB* granite, respectively, and comparison with the ±95 % confidence intervals

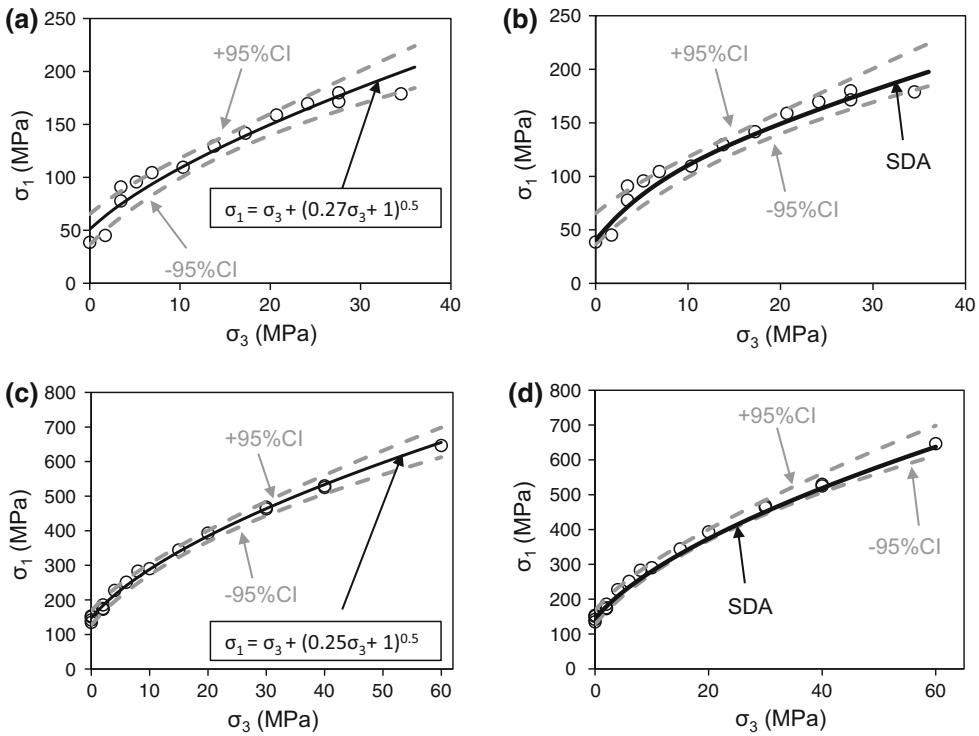

probabilistic analysis of different geotechnical problems. In this article, the concept of confidence intervals was used to assess the prediction quality of the *SDA* for estimating the confined strength of rocks with micro-cracks. It was demonstrated that confined strengths estimated using the *SDA* fall between the ±95 % confidence intervals calculated for the rocks with micro-cracks. Therefore, based on the available data, the results of analyses presented in this article suggest that the *SDA* can provide a reasonable estimate of the confined strength of crack-damaged rocks.

The experimental work by Rosengren and Jaeger (1968) on intact and heat-treated Wombeyan marble was originally conducted to assess the strength properties of heat-treated marble in relation to intact marble to better understand the strength of jointed rock masses as a function of confinement, assuming that the heat-treated marble is an analogue for a highly interlocked jointed rock mass. It was demonstrated in this article that the confined strength of rock specimens with micro-cracks can be estimated using the proposed *SDA*. Further investigation on the applicability of this approach for estimating the confined strength of rocks with larger scale strength dominating features such as veins, fractures and joints is suggested.

7 Summary and Conclusions

The grain-based model previously calibrated to the unconfined and confined strengths of intact and granulated Wombeyan marble by Bahrani et al. (2014) was used to simulate rock specimens with different crack densities. Rock specimens with micro-cracks were simulated by assigning the crack properties to a percentage of the smooth-joint contacts representing the grain boundaries (i.e., $SJ_f = 10$–100 %).

The following can be concluded from the simulation of intact rock and crack-damaged rock specimens:

1. The unconfined and confined strengths of the grain-based specimens with crack density ranging from $SJ_f = 10$ % to $SJ_f = 90$ % are between those of models of intact marble (i.e., $SJ_f = 0$ %) and model of granulated marble (i.e., $SJ_f = 100$ %);
2. The confined strengths of grain-based specimens with micro-cracks increase rapidly with increasing confinement and approach those of intact grain-based specimens at a confining pressure equal to about 10 % of the *UCS* of intact specimen (i.e., $\sigma_3 = UCS_i/10$);
3. The density of cracks does not influence the overall macroscopic failure mode at different levels of confinement: transition from axial fracturing along the grain boundary at low confinement to shear failure through grains at high confinement is observed in all grain-based specimens independent of their initial micro-crack density;
4. At the specimen scale, the failure mode changes from axial splitting at low confinement to shear rupture formation at high confinement and this is independent of the density of cracks;
5. At the grain scale, three modes of failure are opening, combined opening-shearing and shearing;
6. Opening, which occurs along the grain boundaries, is dominant under unconfined conditions, while shearing, which occurs through the grains, is dominant at high confinement ($\sigma_3 > UCS_i/10$).

The simulation results including the unconfined and confined peak strengths of grain-based specimens with various crack densities were used to develop a series of semi-empirical relations, which describe the strength degradation of a rock with micro-cracks from the intact rock as a function of confinement. Therefore, having knowledge of the unconfined and confined strengths of the intact rock and the unconfined strength of the rock containing micro-cracks, the confined strength of the crack-damaged rock can be estimated.

The applicability of this approach, called the strength degradation approach (*SDA*), for estimating the confined strength of rocks with micro-cracks was assessed by comparing it with the published laboratory tests. It follows that the *SDA* provided a reliable estimate of the mean confined strength of rock specimens containing various crack densities.

To the knowledge of the authors, the strength degradation approach (*SDA*) is the only quantitative method to estimate the confined strength of crack-damaged rocks. It is suggested that the applicability of this approach for estimating the confined strength of such rocks and rocks containing larger scale strength dominating features needs further investigations.

Acknowledgments This research project was supported by the Natural Sciences and Engineering Research Council of Canada (*NSERC*), the Centre for Excellence in Mining Innovation (*CEMI*) through the Smart Underground Monitoring and Integrated Technologies (*SUMIT*) program lead by Laurentian University, and the Itasca Consulting Group through its Itasca Education Partnership (*IEP*) program. The authors would like to acknowledge Nezam Bozorgzadeh from University of Toronto for insightful discussions about the statistical concepts and approach used in this article.

Appendix

This Appendix summarizes the terminologies adopted in this article.

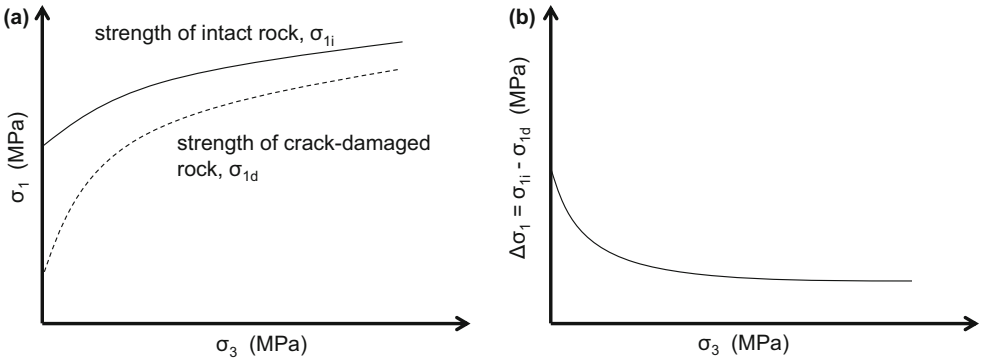

Fig. 16 Schematic representation of: **a** strength envelopes of intact and crack-damaged rocks; and **b** strength degradation of a crack-damaged rock as a function of confinement

Intact Rock

Intact rock is used to describe the homogeneous portion of a rock, the material between geological features, which might be represented by a hand specimen or piece of drill core examined in the laboratory (Brady and Brown 2007). In this article, intact rock refers specifically to a laboratory specimen that does not contain any strength dominating features such as micro-cracks, fractures, veins, or cemented joints.

Micro-cracks

Micro-cracks are noncohesive flaws at the grain scale such as grain and grain boundary cracks, which may influence the strength and/or failure mode of rocks under different stress conditions.

UCS_i and UCS_d

UCS stands for unconfined compressive strength. The value of *UCS* is directly obtained from the laboratory unconfined compression test. In this article, UCS_i and UCS_d are used to describe the unconfined compressive strength of "intact" rock and rock specimens with micro-cracks, respectively.

UCS_i and σ_{ci}

UCS_i is the unconfined compressive strength obtained directly from laboratory tests on unconfined intact rock specimens. As per recommendation by Hoek and Brown (1997), σ_{ci} is determined by extrapolation, from fitting triaxial test data covering a confinement range up to half of UCS_i in five equal increments, to the unconfined state; it is obtained by back projection using a least-square regression analysis. Studies by Kaiser and Kim (2015) have shown that independently determined unconfined strengths from *UCS* tests and from triaxial tests (σ_{ci}) on the same rock type do not correspond; UCS_i is often lower than σ_{ci}. Thus, *UCS* data should not be used as a replacement for σ_{ci}.

Strength Degradation

The term "degradation" in rock mechanics is used for different purposes. For example, Fang and Harrison (2001) used the term "degradation" to describe the post-peak strength reduction. In this article, the difference between the peak strengths of intact rock and rock containing micro-cracks (or the peak strength reduction due to micro-cracks) is called "rock strength degradation." The concept of strength degradation is schematically shown in Fig. 16. Figure 16a illustrates a situation where the strength of a rock with micro-cracks increases rapidly with increasing confinement and approaches the intact strength. Therefore, the strength degradation ($\Delta\sigma_1$), which is the strength difference between the intact rock (σ_{1i}) and the rock with micro-cracks (σ_{1d}), decreases rapidly with increasing confinement and remains almost constant beyond a critical confining pressure (Fig. 16b).

According to Bahrani and Kaiser (2013), this critical confining pressure is between $UCS_i/20$ and $UCS_i/6$, with a typical central value of $UCS_i/10$, as was suggested by Kaiser and Kim (2015). The rapid increase in the strength of rocks containing micro-cracks with confinement is due to the reduction in the length of propagating cracks and a resistance of an interlocked structure to dilation. When the confining pressure is greater than about 10 % of the applied axial stress, ($\sigma_1/\sigma_3 > 0.1$; Hoek and Bieniawski 1965; Diederichs 2003) shear banding or shear rupture starts and eventually dominates the confined rock failure process.

References

Bahrani N, Kaiser PK (2013) Strength degradation of non-persistently jointed rock mass. Int J Rock Mech Min Sci 62:28–33

Bahrani N, Kaiser PK, Valley B (2014) Distinct element method simulation of an analogue for a highly interlocked, non-persistently jointed rock mass. Int J Rock Mech Min Sci 71:117–130

Brady BHG, Brown ET (2007) Rock mechanics for underground mining. Kluwer Academic Publishers, The Netherlands

Diederichs MS (2003) Manuel Rocha medal recipient: rock fracture and collapse under low confinement conditions. Rock Mech Rock Eng 36(5):339–381

Eberhardt E, Stead D, Stimpson B (1999) Effects of sample disturbance on the stress-induced microfracturing characteristics of brittle rock. Can Geotech J 36:239–250

Fang Z, Harrison JP (2001) A mechanical degradation index for rock. Int J Rock Mech Min Sci 38:1193–1199

Gerogiannopoulos NG (1976) A critical state approach to rock mechanics. PhD thesis, University of London

Griffith AA (1921) The phenomena of rupture and flow in solids. Philos Trans R Soc Lond A 221:163–198

Hoek E, Bieniawski ZT (1965) Brittle rock fracture propagation in rock under compression. Int J Fract Mech 1:137–155

Hoek E, Brown ET (1980) Underground excavations in rock. Institution of mining and metallurgy, London

Hoek E, Brown ET (1997) Practical estimates of rock mass strength. Int J Rock Mech Min Sci 34(8):1165–1186

Holt RM, Brignoli M, Kenter CJ (2000) Core quality: quantification of coring-induced rock alteration. Int J Rock Mech Min Sci 37:889–907

Itasca (2008) Particle flow code in 2 dimensions (PFC2D), Ver. 4.0. Itasca Consulting Group Inc, Minneapolis

Kaiser PK, Kim B (2015) Characterization of strength of intact brittle rock considering confinement-dependent failure processes. Rock Mech Rock Eng 48(1):107–119

Lanaro F, Sato T, Nakama S (2009) Depth variability of compressive strength test results of Toki granite from Shobasama and Mizunami Construction Sites, Japan. Rock Mech Rock Eng 42:611–629

Martin C (1993) The strength of massive Lac du Bonnet granite around underground openings. PhD thesis, University of Manitoba

Martin CD, Stimpson B (1994) The effect of sample disturbance on laboratory properties of Lac du Bonnet granite. Can Geotech J 31:692–702

Patton FD (1966) Multiple mode of shear failure in rock. In: 1st international conference Rock Mech, Lisbon, pp 509–511

Potyondy DO (2010) A grain-based model for rock: approaching the true microstructure. In: Proceeding of Rock Mech in the Nordic Countries

Potyondy DO, Cundall PA (2004) A bonded particle model for rock. Int J Rock Mech Min Sci 41:1329–1364

Rosengren KJ, Jaeger JC (1968) The mechanical properties of an interlocked low-porosity aggregate. Géotechnique 18:317–326

Watson BP, Kuijpers JS, Henry G, Palmer CE, Ryder JA (2009) Nonlinear rock behaviour and its implications for deeper level platinum mining. J South Afr Inst Min Metall 108:5–13